Environmental Science & Technology

pubs.acs.org/est

Article

Isotopic Interpretation of Particulate Nitrate in the Metropolitan City of Karachi, Pakistan: Insight into the Oceanic Contribution to NO_x

Zheng Zong, Chongguo Tian,* Jun Li,* Jabir Hussain Syed, Wei Zhang, Yunting Fang, Yifan Jiang, Jawad Nasir, Muhammad Mansha, Syed Hussain Haider Rizvi, Muhammad Shafiq, Suhaib Bin Farhan, and Gan Zhang

Cite This: *Environ. Sci. Technol.* 2020, 54, 7787−7797

Read Online

ACCESS | Metrics & More | Article Recommendations | Supporting Information

ABSTRACT: Nitrogen oxide (NO_x) abatement has become the focus of air quality management strategies. In this study, we examined NO_x sources and the atmospheric conversion of NO_x in Karachi, Pakistan, a megacity in South Asia with serious particulate pollution problems. Oceanic contributions to NO_x were quantified for the first time based on a novel approach using nitrogen/oxygen isotopic analysis in nitrate ($\delta^{15}N-NO_3^-$; $\delta^{18}O-NO_3^-$) and a Bayesian model. Our results showed that $\delta^{15}N-NO_3^-$ in Karachi varied between −10.2‰ and +12.4‰. As indicated by the $\delta^{18}O-NO_3^-$ findings (+66.2 ± 7.8‰), the •OH pathway dominated NO_x conversion throughout the nearly two-year observation, but high NO_3^- events were attributed to the O_3 pathway. Coal combustion was the most significant source (32.0 ± 9.8%) of NO_x in Karachi, with higher contributions in the autumn and winter; a similar situation occurred for biomass burning + lightning (30.3 ± 6.5%). However, mobile sources (25.2 ± 6.4%) and microbial processes (12.5 ± 7.5%) exhibited opposite seasonal trends. The oceanic contributions to NO_x in Karachi were estimated to be 16.8%, of which lightning, shipping emissions, and microbial processes accounted for 20.3%, 46.3%, and 33.4%, respectively, emphasizing the dominance of shipping emissions as an oceanic NO_x source.

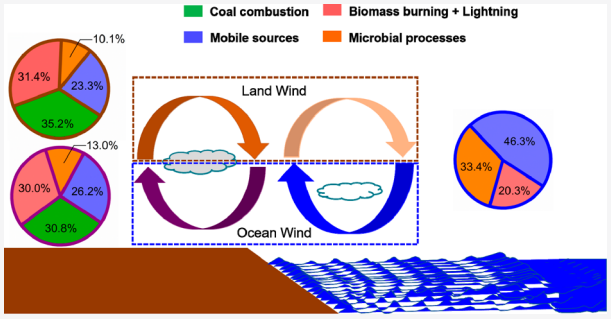

INTRODUCTION

Nitrogen oxides (NO_x, consisting mainly of NO and NO_2) make up a large proportion of the reactive nitrogen and are the main precursors of particulate nitrate (NO_3^-) in the atmosphere.[1] NO_x is thought to be closely linked to a wide range of environmental issues, including ozone problems, acid rain, soil acidification, and increasingly serious particulate pollution (Supporting Information SI, Text S1).[2−4] Thus, NO_x abatement has become the focus of pollution control and quantitative analysis of its emission a premise of governance. Generally, NO_x is emitted from a wide range of sources, including biomass burning, fossil energy consumption (e.g., coal combustion, vehicle exhaust, and shipping emissions), microbial processes, and lightning.[5] These sources include emissions occurring over the terrain and ocean, respectively; however, presently, few source-parsed researches have been conducted and were typically focused on the former.[6] In fact, oceanic sources, such as shipping emissions, lightning in ocean areas, and microbial processes in marine sediment and estuaries, are important contributors to NO_x emissions, especially in areas affected by ocean winds.[6,7] Globally, about 15% of the world's NO_x is emitted from oceangoing ships, and 5%−15% can be attributed to lightning.[8] A simulation by Ding et al. indicated that shipping emissions contribute up to 5%−20% to local NO_x concentrations in densely populated coastal regions of China.[9] Therefore, the insufficient analysis of NO_x sources, especially quantifying the contributions of oceanic ones, complicates the mitigation efforts of NO_x pollution.

Several methods for apportioning NO_x emissions have been accepted, such as air quality models and satellite observations.[9,10] However, each is accompanied by certain imperfections. As for air quality models, parameter setting could lead to source contributions that can differ in magnitude. A comparative study shows that for a particular data set the CAMx model results are usually 10%−20% higher than that of CMAQ.[10] In satellite observations, it is still difficult to relate NO_x emissions to the derivative patterns (e.g., atmospheric

Received: January 23, 2020
Revised: May 8, 2020
Accepted: June 3, 2020
Published: June 3, 2020

NO_3^- concentration and deposition) due to their extended lifetimes relative to NO_x, which restricts its application. Compared with these simulations, the real-measured methods may better resolve the uncertainty in source apportionment of NO_x. The nitrogen isotope technique using atmospheric-derived nitrate ($\delta^{15}N-NO_3^-$) has been applied extensively to track NO_3^- and NO_x because the nitrogen isotopic signature of different NO_x sources generally varies over a large range.[11−14] The technology roughly originated in the 1950s and was mainly applied to the source analysis of NO_3^- in rainwater.[15−17] For example, based on the feature of $\delta^{15}N-NO_3^-$, Hoering postulated that NO_3^- in rain partly arose from the oxidation of ammonia.[18] With the need of environmental governance, sources of NO_3^- in aerosols are gradually apportioned by this technology, and NO_3^- targets also vary from TSP to PM_{10} to $PM_{2.5}$.[14,19−23] For more detailed historical researches, please refer to SI Text S2 and Elliott et al.[24] In addition, $\delta^{15}N-NO_3^-$ analysis results have steadily moved from qualitative to quantitative assessment. This progress is attributable to (i) continuous enrichment of the actual $\delta^{15}N-NO_x$ source values detected,[25−30] (ii) quantification of isotope fractionation that occurs with the conversion of NO_x to NO_3^-,[31,32] and (iii) the application of isotopic mixing models.[33] In this context, the ability to quantify comprehensive $\delta^{15}N-NO_3^-$ analysis results (including the terrestrial and oceanic nature) is expected to facilitate mitigation and management efforts to reduce NO_x pollution levels.

South Asia is experiencing serious air quality issues (particulate pollution), resulting in a significant rise in health-related morbidity with chronic exposure to air pollution.[34] Thereinto, Karachi, a metropolitan city in Pakistan with a population of 14.9 million (2017 Census) is the representative city. Khan et al. reported that daily concentrations of particulate matter with diameters less than 2.5 μm ($PM_{2.5}$) approached 177.4 $\mu g\ m^{-3}$, averaging levels 4−10-fold higher than World Health Organization guidelines.[35] Khwaja et al. revealed sobering morbidity rates among an estimated population of 15 million as a result poor air quality.[36] These data highlight the urgency of taking immediate measures to address the air pollution problem in Karachi. However, the research still lacks data on the source characteristics of NO_x ,and native $\delta^{15}N-NO_3^-$ remains poorly understood at Karachi, and even South Asia (SI Text S3). These deficiencies have limited the ability to enact measures to control indigenous air pollution there. Additionally, Karachi is located on the coast between the Arabian Sea (AS) and South Asian continent (SAC), characterized by sea−land breezes and prevailing northeast and southwest winds.[37] This makes Karachi, a typical coastal city, susceptible to mixed sources of air pollution, both terrestrial and oceanic in nature.

In response to the insufficient comprehension on the sources of NO_3^- or NO_x in Karachi, this study conducts a nearly 2-year sampling of particulate matter. The objectives are to (i) explore the annual, seasonal, and diurnal variations in NO_3^-, (ii) investigate the sources and conversion features of NO_x using nitrogen/oxygen isotopic analysis ($\delta^{15}N-NO_3^-$, $\delta^{18}O-NO_3^-$), (iii) quantitatively apportion the year-round NO_x sources relying on a Bayesian mixing model, and (iv) quantify the contribution of oceanic sources to NO_x emissions based on a derivative approach. This study aims to originally reveal the $\delta^{15}N-NO_3^-$ at Karachi in South Asia and to apportion the source of precursory NO_x. In addition, the results from this study are expected to pave the way to quantify oceanic sources of NO_x in coastal regions.

■ MATERIALS AND METHODS

Sampling Campaign. Sampling of total suspended particulates was conducted in Karachi (24°51′ N; 67°02′ E) from 2 February 2016 to 23 November 2017. The sampling point is on the top floor of an office building of a government agency (about 12 m in height), which is located in the west of Karachi, on the edge of the main district (SI Figure S1). No agricultural land, but some semiarid bushes, surround it. In addition, there are some government departments gathering here, where no nearby anthropogenic NO_x sources are apparent. Samples were collected using a glass fiber filter and a high-volume sampler (KC-1000, Longtuo) at a flow rate of 1.13 $m^3\ min^{-1}$. The diurnal sampling (12/12 h; day: 10:00 am−22:00 pm; night: 22:00 pm−10:00 am, local time) was carried out once a week every month. In total, 159 samples were collected over the sampling campaign. To minimize contamination, all filters were preheated at 450 °C for 6 h in a muffle furnace before sampling. After sampling, the filters were folded and stored in a refrigerator (−20 °C) until further analysis.

The synoptic system in Karachi was dominated by southwest and northeast winds. Here, 70% (B1:11% + B2:59%; SI Figure S2) of the backward trajectories, i.e., from the ocean to the land, originated from the AS; the remaining 30% (B3) came from the SAC. For the forward trajectories (i.e., from the land to the ocean), 69% (F1:39% + F2:30%) of the air mass continued to move over terrain areas, and 31% (F3:13% + F4:18%) was transferred to the ocean. Such interactions between the land and ocean enable pollutant transfer and exchange, leading to mixed-source air pollution in Karachi.

Chemical and Isotopic Analysis. For NO_3^- species, briefly, a punch cutout (diameter: 47 mm) was removed from the sample collection filter and immersed in Milli-Q water. Samples were extracted ultrasonically for 20 min, and the extracts were filtered. NO_3^- concentration was measured using an ion chromatograph (Dionex ICS3000, Thermo Fisher Scientific).[38] The detection limit was 10 ng mL^{-1} with less than a 5.2% error. The nitrous oxide (N_2O) isotopic procedure was applied to quantify $\delta^{15}N-NO_3^-$ and $\delta^{18}O-NO_3^-$ (n = 159).[39] In brief, NO_3^- extract was diluted to 15 μmol L^{-1} in a 5 mL solution with 0.5 mol L^{-1} NaCl. Then, 0.3 g of cadmium powder was added to the solution, and its pH was adjusted to 9 by injecting 0.1 mL of imidazole (1 mol L^{-1}). Capped tightly with rubber septa, the processed samples were ultrasonically oscillated for 2 h at 40 °C. In this study, the reduction rate of NO_3^- to NO_2^- by cadmium reduction was 97.8% ± 8.3%. After normalizing for 12 h, 4 mL of reacted solution was transferred to a new sample bottle. Sodium azide (1:1 of 20% acetic acid and sodium azide, purged with helium at 70 mL min^{-1} for 10 min) was injected for a 30 min reaction. Finally, the reaction was stopped by 0.4 mL of 10 mol L^{-1} NaOH. The isotopes $\delta^{15}N$ and $\delta^{18}O$ of N_2O were analyzed using an isotope ratio mass spectrometer (MAT253, Thermo Fisher Scientific). The values of $\delta^{15}N-NO_3^-$ and $\delta^{18}O-NO_3^-$ are reported in parts per thousand relative to the standard guidelines (IAEA-NO-3, USGS32, USGS34, and USGS35)

$$\delta^{15}N = [(^{15}N/^{14}N)_{sample}/(^{15}N/^{14}N)_{standard} - 1] \times 1000 \quad (1)$$

https://dx.doi.org/10.1021/acs.est.0c00490
Environ. Sci. Technol. 2020, 54, 7787−7797

$$\delta^{18}O = [(^{18}O/^{16}O)_{sample}/(^{18}O/^{16}O)_{standard} - 1] \times 1000 \quad (2)$$

Analytical precision, as calculated using replicates, was less than 0.4‰ for $\delta^{15}N-NO_3^-$ and 0.6‰ for $\delta^{18}O-NO_3^-$. The concentrations of NO_2^- were mostly lower than the detection limit and less than 0.2% of NO_3^-, which were ignored during the isotopic analyses. The NO_3^- concentration for each sample was recalculated by subtracting the average blank value; $\delta^{15}N-NO_3^-$ and $\delta^{18}O-NO_3^-$ was determined for each sample by mass balance (SI Text S4).

Monte Carlo Simulation. Monte Carlo simulation refers to a method that uses random or pseudorandom numbers to solve many calculation problems.[40] Its process is to construct the estimated value of the unknown quantity to be obtained by sampling the random number x_i (i = 1, 2, . . ., N). The main theoretical basis is the central-limit theorem

$$\frac{\sqrt{N}(\frac{1}{N}\sum_{i=1}^{N} x_i - \mu)}{\sigma} \sim N(0, 1) \quad (3)$$

where x_i is the random number, μ and σ represent the mean and standard deviation, respectively, and N tends to infinity. In this study, the Monte Carlo method was performed to get the feasible solutions of the Bayesian mixing model and the module for qualifying oceanic contributions, respectively.

Bayesian Mixing Model. Source apportionment of NO_x in Karachi was resolved using an improved Bayesian mixing model. Except for the basic Bayesian principle,[41] this model was perfected by incorporating the isotopic fractionation of the equilibrium/Leighton reaction during the conversion of NO_x to NO_3^-. Briefly, isotopic fractionation can be regarded as the mixed contribution of two dominative transformations from NO to HNO_3 (neglecting the isotope fractionation from HNO_3 to NO_3^-).[32] The first transformation is the oxidizing reaction from NO to NO_2 and the reaction from NO_2 to HNO_3 by photochemically produced •OH, as abbreviated by the •OH pathway. The second involves the oxidizing reaction from NO to NO_2, an NO_3 radical by O_3, and the hydrolysis reaction of N_2O_5 on a wetted surface to form HNO_3, i.e., the H_2O pathway. Thus, the nitrogen isotopic fractionation contributed by transformation from NO to HNO_3 via both the •OH and H_2O pathways can be represented as

$$\Delta[\delta^{15}N - NO_3^-] = \gamma \times \Delta[\delta^{15}N - NO_3^-]_{OH} + (1-\gamma) \times \Delta[\delta^{15}N - NO_3^-]_{H_2O} \quad (4)$$

where $\Delta[\delta^{15}N-NO_3^-]_{OH}$ and $\Delta[\delta^{15}N-NO_3^-]_{H2O}$ represent the differences in the nitrogen isotope composition between HNO_3 (NO_3^-) and NO caused by the •OH and H_2O pathways, respectively. Assuming no kinetic isotopic fractionation associated with the reaction between NO_2 and •OH, $\Delta(\delta^{15}N\text{-}HNO_3)$ and $\Delta(\delta^{15}N\text{-}HNO_3)_{H2O}$ can be calculated using mass balance, respectively, as follows

$$\Delta(\delta^{15}N - HNO_3)_{OH} = \Delta(\delta^{15}N - NO_2)_{OH} = 1000 \times \left[\frac{(^{15}\alpha_{NO_2/NO} - 1)(1 - f_{NO_2})}{(1 - f_{NO_2}) + (^{15}\alpha_{NO_2/NO} \times f_{NO_2})}\right] \quad (5)$$

$$\Delta(\delta^{15}N - HNO_3)_{H_2O} = \Delta(\delta^{15}N - N_2O_5)_{H_2O} = 1000 \times (^{15}\alpha_{N_2O_5/NO_2} - 1) \quad (6)$$

where $^{15}\alpha_{NO2/NO}$ is the equilibrium isotopic fractionation factor between NO_2 and NO, and $^{15}\alpha_{N2O5/NO2}$ refers to the equilibrium isotopic fractionation factor between N_2O_5 and NO_2, which are all temperature-dependent functions (eq 10; SI Table S1).[31] f_{NO2} is the fraction of NO_2 in the total NO_x, typically ranging from 0.2 to 0.95.[42] γ is the contribution of the •OH pathway; its variable range for a specified sample can be assessed by $\delta^{18}O-NO_3^-$ in the sample formed by the •OH and H_2O pathways

$$[\delta^{18}O - NO_3^-] = \gamma \times [\delta^{18}O - NO_3^-]_{OH} + (1-\gamma) \times [\delta^{18}O - NO_3^-]_{H_2O} \quad (7)$$

where $[\delta^{18}O-NO_3^-]_{OH}$ and $[\delta^{18}O-NO_3^-]_{H2O}$ represent $\delta^{18}O-NO_3^-$ formed by the •OH and H_2O pathways, respectively. The $[\delta^{18}O\text{-}NO_3^-]_{OH}$ can be further expressed as[32]

$$[\delta^{18}O - HNO_3]_{OH} = \frac{2}{3}[(\delta^{18}O - NO_2)]_{OH} + \frac{1}{3}[\delta^{18}O - OH]_{OH} = \frac{2}{3}\left[\frac{1000 \times (^{18}\alpha_{NO_2/NO} - 1)(1 - f_{NO_2})}{(1 - f_{NO_2}) + (^{18}\alpha_{NO_2/NO} \times f_{NO_2})} + [\delta^{18}N - NO_x]\right] + \frac{1}{3}[(\delta^{18}O - H_2O) + 1000 \times (^{18}\alpha_{OH/H_2O} - 1)] \quad (8)$$

and $[\delta^{18}O\text{-}NO_3^-]_{H2O}$ can be determined as follows

$$[\delta^{18}O - HNO_3]_{H_2O} = \frac{5}{6}(\delta^{18}O - N_2O_5) + \frac{1}{6}(\delta^{18}O - H_2O) \quad (9)$$

where $^{18}\alpha_{NO2/NO}$ and $^{18}\alpha_{OH/H2O}$ are the equilibrium isotope fractionation factors between NO_2 and NO, and •OH and H_2O, respectively, which are temperature-dependent functions (SI Table S1).

$$1000(^{m}\alpha_{X/Y} - 1) = \frac{A}{T^4} \times 10^{10} + \frac{B}{T^3} \times 10^8 + \frac{C}{T^2} \times 10^6 + \frac{D}{T} \times 10^4 \quad (10)$$

On the basis of the computing theory, a Monte Carlo simulation was performed to generate 10,000 feasible solutions, which determined that the error between predicted and measured $\delta^{18}O$ was less than 0.5‰. For the particular model framework and computing method, readers are referred to Zong et al.[43]

In this study, coal combustion (+13.7 ± 4.6‰),[25,44] biomass burning + lightning (+0.9 ± 3.9‰),[18,26] mobile sources (−7.2 ± 7.4‰),[28,29,44,45] and microbial processes (−35.4 ± 10.7‰)[27,30,46,47] were considered end members in our Bayesian simulation (SI Text S5; Figure S3; Table S2). The Bayesian mixing model was run for four patterns, specifically as overall, seasonal, monthly, and clustering simulations, to investigate the comprehensive NO_x sources in Karachi.

Module for Qualifying Oceanic Contributions. To distinguish the oceanic contribution from Bayesian modeling source apportionment, this model was further modified by adding a module for sample sectionalization and an analytical module (Figure 1). The grouping module was divided into several sample subgroups according to the cluster data of the backward trajectories operated by the HYSPLIT model. The

https://dx.doi.org/10.1021/acs.est.0c00490
Environ. Sci. Technol. 2020, 54, 7787−7797

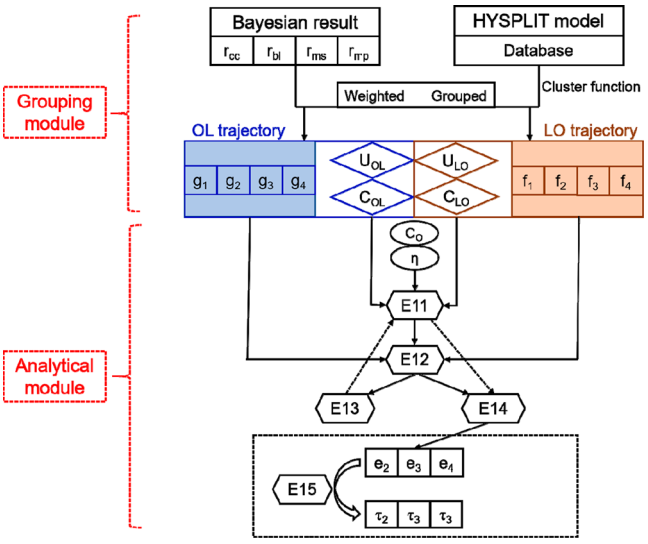

Figure 1. Principle and process of the calculation for oceanic NO_x sources in this study; r_i refers to the contribution proportion of i source from the Bayesian result (cc: coal combustion; bl: biomass burning + lightning; ms: mobile sources; mp: microbial processes); E11−E15 represents formulas 11−15, respectively; other parameters are consistent with their meaning in the text.

HYSPLIT model is a complete system for computing simple air parcel trajectories to complex dispersion simulation.[48] It is available on the National Oceanic and Atmospheric Administration Air Resource Laboratory website (www.arl.noaa.gov/ready/hysplit4.html). In this study, the model was adopted to generate 72 h forward and backward trajectories encountered (500 m) with 6 h intervals at Karachi (SI Text 6). The obtained 318 trajectories were then bunched into clusters by the clustering function of this model. In Karachi, there are four trajectories related to ocean areas (SI Figure S2): two backward trajectories from the ocean to the land (B1 and B2, referred to as the OL trajectory) and two forward trajectories from the land to the ocean (F3 and F4, the LO trajectory). Source contributions from the four Bayesian scenarios were weighted to distinguish the oceanic contribution in subsequent analytical modules.

On the basis of the terrestrial source nature of NO_3^- in the OL trajectory in Karachi (SI Text S7), the NO_3^- flux of the OL trajectory is approximately equal to the product of the sum of the concentration of NO_3^- in the LO trajectory undergoing removal processes (e.g., atmospheric deposition) and the concentration of NO_3^- originating from the ocean and the corresponding wind speed

$$F_{OL} = U_{OL}C_{OL} = U_{LO}[(1-\eta)C_{LO} + C_O] \tag{11}$$

where F_{OL}, U_{OL}, and C_{OL} represent the flux of NO_3^-, the wind speed, and the concentration of NO_3^- in the OL trajectory, respectively. U_{LO} and C_{LO} refer to the wind speed and the concentration of NO_3^- in the LO trajectory, respectively. η is the removal efficiency of NO_3^- from the atmosphere, and C_O is the concentration of NO_3^- emitted by the ocean. According to the results of the Bayesian model, we can resolve the contributions of the four types of emission sources (coal combustion, biomass combustion + lightning, mobile sources, and microbial processes) into C_{OL} and C_{LO}. Of these, only coal combustion shows a pure terrestrial nature; thus, its oceanic contribution would be zero. Equation 11 can be decomposed into the following

$$\begin{aligned}
F_{OL}(C) &= U_{OL}C_{OL}g_1 = U_{LO}(1-\eta)C_{LO}f_1 \\
F_{OL}(B) &= U_{OL}C_{OL}g_2 = U_{LO}[(1-\eta)C_{LO}f_2 + C_O e_2] \\
F_{OL}(T) &= U_{OL}C_{OL}g_3 = U_{LO}[(1-\eta)C_{LO}f_3 + C_O e_3] \\
F_{OL}(V) &= U_{OL}C_{OL}g_4 = U_{LO}[(1-\eta)C_{LO}f_4 + C_O e_4]
\end{aligned} \tag{12}$$

where $F_{OL}(C)$, $F_{OL}(B)$, $F_{OL}(T)$, and $F_{OL}(V)$ refer to the NO_3^- flux contributed by coal combustion, biomass combustion + lightning, mobile sources, and microbial processes, respectively, in the OL trajectory; g_1, g_2, g_3, and g_4 are the contribution ratios for coal combustion, biomass combustion + lightning, mobile sources, and microbial processes, respectively, in the OL trajectory; f_1, f_2, f_3, and f_4 are the contribution ratios for coal combustion, mobile sources, biomass combustion + lightning, and microbial processes, respectively, in the LO trajectory; and e_2, e_3, and e_4 refer to the contribution ratios of biomass combustion + lightning, mobile sources, and microbial processes from marine sources, respectively. In light of the pure terrestrial nature of coal combustion, the parameter η can be transformed into

$$\eta = 1 - \frac{U_{OL}C_{OL}g_1}{U_{LO}C_{LO}f_1} \tag{13}$$

From the formulas given, C_O, e_2, e_3, and e_4, are given by

$$\begin{aligned}
C_O &= \left(1 - \frac{g_1}{f_1}\right)\frac{U_{OL}C_{OL}}{U_{LO}} \\
e_2 &= \left(g_2 - \frac{g_1}{f_1}f_2\right)\Big/\left(1 - \frac{g_1}{f_1}\right) \\
e_3 &= \left(g_3 - \frac{g_1}{f_1}f_3\right)\Big/\left(1 - \frac{g_1}{f_1}\right) \\
e_4 &= \left(g_4 - \frac{g_1}{f_1}f_4\right)\Big/\left(1 - \frac{g_1}{f_1}\right)
\end{aligned} \tag{14}$$

The formulas can be further used to calculate the contributions of biomass combustion + lightning (τ_2), mobile sources (τ_3), microbial processes (τ_4), and their sum (τ_T)

$$\begin{aligned}
\tau_T &= \frac{C_O}{C_{OL}} = \left(1 - \frac{g_1}{f_1}\right)\frac{U_{OL}}{U_{LO}} \\
\tau_2 &= \left(g_2 - \frac{g_1 f_2}{f_1}\right)\frac{U_{OL}}{U_{LO}} \\
\tau_3 &= \left(g_3 - \frac{g_1 f_3}{f_1}\right)\frac{U_{OL}}{U_{LO}} \\
\tau_4 &= \left(g_4 - \frac{g_1 f_4}{f_1}\right)\frac{U_{OL}}{U_{LO}}
\end{aligned} \tag{15}$$

It is noted that the mean values and the associated standard deviations (mean ± SD) were employed consistently throughout the modeling operation. Arithmetically, a Monte Carlo simulation was performed to generate 10,000 feasible

https://dx.doi.org/10.1021/acs.est.0c00490
Environ. Sci. Technol. 2020, 54, 7787−7797

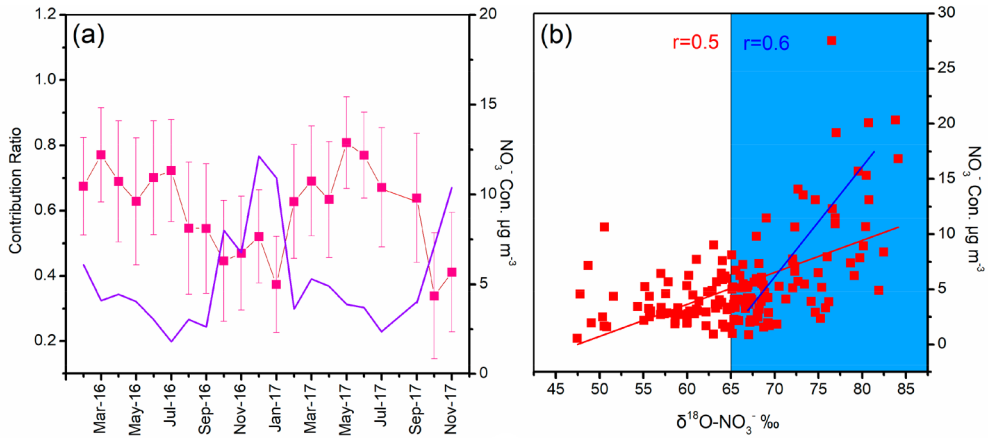

Figure 2. (a) Relationship between calculated •OH pathway ratio (pink box; mean ± standard) and NO_3^- concentration (purple line). (b) Correlation coefficients between $\delta^{18}O-NO_3^-$ and NO_3^- concentration (overall correlation and correlation when limiting $\delta^{18}O-NO_3^-$ to +65‰ or more).

solutions (SI Figure S4), and an iterative model with a simulation step of 0.01 was applied to achieve optimal results.[49]

RESULTS AND DISCUSSION

Concentration Regime and Source Feature Based on $\delta^{15}N-NO_3^-$. From February 2016 to November 2017, the concentration of NO_3^- ranged from 0.6 to 27.5 $\mu g\ m^{-3}$ in Karachi, with a mean value of 5.4 ± 4.1 $\mu g\ m^{-3}$. Compared with previous studies, our results indicated an increase in the NO_3^- concentration, which was attributed to population expansion and enhanced energy consumption.[50,51] The daytime concentration (5.8 ± 4.7 $\mu g\ m^{-3}$) was comparable to the concentration at night (5.2 ± 3.2 $\mu g\ m^{-3}$) with no significant difference. However, a distinct seasonal variation was observed, with higher values ($p < 0.01$) in the autumn and winter (average: 7.1 ± 5.1 $\mu g\ m^{-3}$) and lower values in summer and spring (average: 3.9 ± 2.0 $\mu g\ m^{-3}$). Specifically, the highest concentrations occurred in November, December, and January, and the lowest values in June, July, and August (SI Figure S5; Table S3). Annually, the second study year exhibited higher values than the first, which is consistent with the worsening trend of pollution in South Asia.[52]

Pollutant concentrations are generally governed by meteorological conditions and emission sources.[53] The temperature and relative humidity shared an insignificant correlation with NO_3^- concentrations, indicating a weak impact of these meteorological parameters on the variation of NO_3^-. Nonetheless, the NO_3^- concentrations were positively correlated with wind speed, with r of 0.5 ($p < 0.05$). It suggests that the influence of wind speed was stronger than other meteorological parameters. In addition, $\delta^{15}N-NO_3^-$ reflected the changing character of potential NO_x source types. During the observing period, $\delta^{15}N-NO_3^-$ varied between −10.2‰ and +12.4‰, with a mean value of +1.8 ± 4.5‰ (SI Figure S6). Compared with the readings obtained at night (+1.4 ± 4.0‰), there is no significant difference in the value of $\delta^{15}N-NO_3^-$ for the daytime (+2.1 ± 4.9‰; $p > 0.05$), similar to the stable tendency of the NO_3^- concentration. In autumn and winter, the average $\delta^{15}N-NO_3^-$ reading was +3.1 ± 3.9‰, which was significantly higher ($p < 0.01$) than that for spring and summer (−0.2 ± 3.1‰). Atmospheric NO_3^- is derived mainly from the oxidation of NO_x, whereas the $\delta^{15}N-NO_x$ from different anthropogenic or natural sources shows great variability.[26,30] For example, NO_x from coal combustion has a higher ^{15}N value (+13.7 ± 4.6‰),[25] whereas $\delta^{15}N-NO_x$ from microbial processes is often negative (−35.4 ± 10.7‰).[27] Despite the ^{15}N isotopic fractionation that occurs in the conversion of NO_x to NO_3^-, a previous study has indicated that NO_x sources can be identified based on the $\delta^{15}N-NO_3^-$ value.[54] In this study, we corrected the corresponding $\delta^{15}N-NO_x$ by removing the potential isotopic fractionation (SI Figure S6), manifesting a parallel trend with $\delta^{15}N-NO_3^-$. As such, the observed variation in $\delta^{15}N-NO_3^-$ at Karachi can be linked to an increase in coal combustion in the autumn and winter and to microbial processes in the spring and summer, which could be further verified by the subsequent results of the Bayesian model.

Formation Pathway of NO_x Inferred from $\delta^{18}O-NO_3^-$. In the atmosphere, the main conversion processes of NO_x to NO_3^- (SI SR_1-SR_8) include the •OH pathway (SI SR_4) and O_3 pathway (SI SR_5-SR_7). Thus, $\delta^{18}O-NO_3^-$ can be used to determine NO_x conversion trends, given that the reported $\delta^{18}O-H_2O$ readings ranged from −25‰ to 0‰, showing a significant difference with respect to $\delta^{18}O-O_3$ readings (+90‰ to +122‰).[3] The HC/DMS pathway (NO_3 + DMS/HC reactions) is also an important conversion pathway of NO_x to NO_3^-, especially in the high latitudes in the marine boundary layer.[55] Limited to the lack of $\Delta^{17}O$ data, its proportion in the NO_x conversion could not be quantified here. However, its contribution should be small due to the geographical location of Karachi (SI Figure S7).[56] Therefore, this pathway was ignored in this study, which may cause some uncertainty to the result. In Karachi, the average for $\delta^{18}O-NO_3^-$ was +66.2 ± 7.8‰, ranging from +47.5‰ to +84.1 ‰ (SI Figure S8), well within the broad range of values reported previously.[11,57] Thus, the results revealed a seasonal trend, with higher ($p < 0.05$) values in autumn and winter (average: + 69.0 ± 8.6‰) than in spring and summer (average: + 63.6 ± 5.7‰); this suggests the prevalence of the O_3 pathway in cold seasons. Unlike the results from other studies,[38] no significant diurnal variation in $\delta^{18}O-NO_3^-$ was observed ($p > 0.05$, + 65.6 ± 10.1‰ and +66.6 ± 7.8‰ during the day and at night, respectively), indicating no obvious change in the NO_3^-

https://dx.doi.org/10.1021/acs.est.0c00490
Environ. Sci. Technol. 2020, 54, 7787−7797

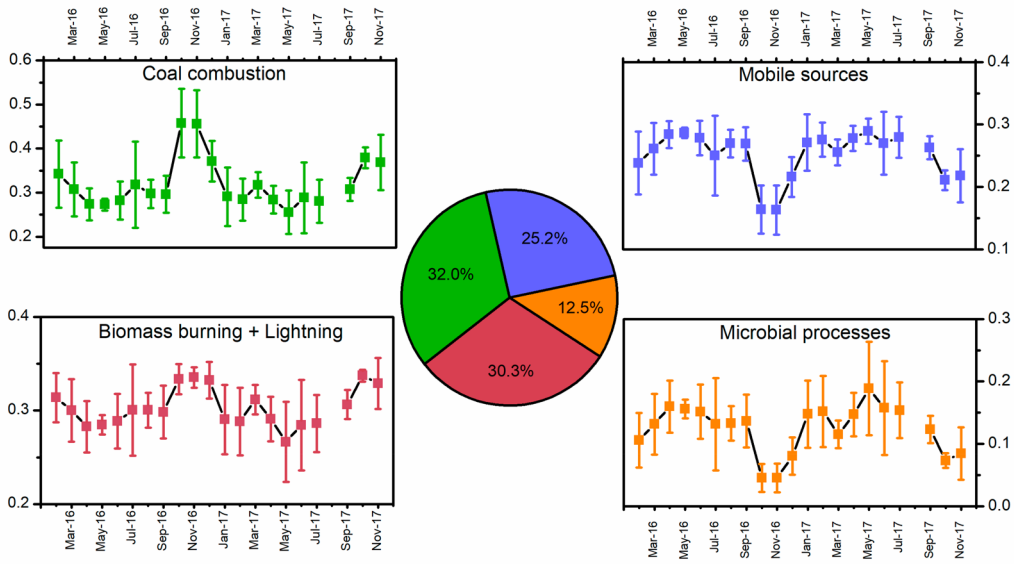

Figure 3. Contributions of coal combustion, mobile sources, biomass burning + lightning and microbial processes to NO_x at Karachi.

generation pathway over the course of a 24-h period. This may be related to the high average temperature (27.1 ± 4.2 °C) throughout the study period, showing only slight diurnal variation. For the O_3 pathway, nitrogen pentoxide (N_2O_5; SI SR_6) is the key intermediate; its thermolabile character reduced the influence of the O_3 pathway during the nighttime hours in this study compared with results previously reported.[58]

To further quantify the ratio of the two NO_x conversion processes, we applied certain assumptions (2/3 of oxygen atoms in NO_3^- are from O_3 and 1/3 from •OH in the •OH pathway, and 5/6 of oxygen atoms are from O_3 and 1/6 from •OH in the O_3 pathway) to the Bayesian mixing model and estimated the respective ratio using a Monte Carlo simulation.[3] The mean and standard deviations of the contribution for the •OH pathway are presented in Figure 2(a). Overall, the wide range (20.3%−94.9%) was due to the broad range of $\delta^{18}O-O_3$ (+90‰ to +122‰) and $\delta^{18}O-$•OH values (−25‰ to 0‰) used; however, the mean values showed distinct seasonal fluctuations. The average contribution of the •OH pathway in autumn and winter was 52.1 ± 28.4% and that in spring and summer was 69.9 ± 14.2%. Thus, the proportion of the •OH pathway in autumn and winter was about 17.8% lower than that in the spring and summer when the •OH conversion pathway was absolutely dominant. No significant diurnal variation was observed, with contributions of 62.0 ± 21.4% in the daytime and 60.5 ± 22.5% at night. These values were both consistent with $\delta^{18}O-NO_3^-$ trends discussed earlier. In addition, the •OH pathway proportion showed a strong negative correlation with NO_3^- concentration ($r = 0.6$, $p < 0.01$). This implies that O_3 may be the major contributing factor to high NO_3^- concentrations in Karachi, as further indicated by the correlation coefficient between $\delta^{18}O-NO_3^-$ and the NO_3^- concentration (Figure 2b).[59] The correlation coefficient was 0.5 but increased to 0.6, limiting $\delta^{18}O-NO_3^-$ to +65‰ or more. $\delta^{18}O-O_3$ ranged from +90‰ to +122‰; higher $\delta^{18}O-NO_3^-$ values denote a stronger effect by O_3. Thus, we can conclude that although the •OH pathway dominated the NO_x conversion in Karachi, the high NO_3^- concentration indicates a strong effect related to the O_3 pathway. Thus, controlling O_3 emissions may be an effective measure to reduce the indigenous occurrence of high pollution events.[60]

Source Apportionment of NO_x Based on the Bayesian Mixing Model. The overall simulation results showed that coal combustion was the most significant source (32.0 ± 9.8%) of NO_x in Karachi, followed by biomass burning + lightning (30.3 ± 6.5%), mobile sources (25.2 ± 6.4%), and microbial processes (12.5 ± 7.5%). These findings are consistent with Karachi's characteristic forms of energy consumption.[61] To our knowledge, no studies have been conducted on the analysis of NO_3^- or NO_x using nitrogen isotopes in South Asia (SI Text S3), which greatly hinder the regional comparison. Therefore, this study selects Beijing, one of the most polluted megacity cities in China, as a comparison object to further analyze the source characteristics of NO_x at Karachi. The comparison between the two cities could reflect the pollution status of China and Pakistan, in East Asia and South Asia, respectively. Compared with Beijing [evaluated by the same method: coal combustion (40.5 ± 12.3%), biomass burning (21.5 ± 5.8%), vehicle exhausts (24.1 ± 3.8%), and the microbial N cycle (14.0 ± 7.5%)], the contributions of coal combustion and microbial processes were lower (SI Figure S9); however, mobile sources and biomass burning + lightning were higher. Although Karachi is a megacity, biomass is the main contributor to NO_x emissions in slum areas located throughout the city. Alam et al. reported that household combustion emission comprised mainly biomass burning, an important contributor to PM_{10} in Pakistan.[62] In Lahore and Karachi, biomass and coal combustion have been shown to contribute greatly to secondary aerosol formation, especially NO_3^- and SO_4^{2-}.[63,64] In another study, 24-h levoglucosan analysis indicated an average reading of 535 ng m^{-3} in Karachi from the burning of various hardwoods and softwoods.[35] In addition, Chen et al. reported that lightning sources contributed up to 56% of the NO_3^- emissions in wet deposition in Zhanjiang, a tropical city in China with a similar latitude to Karachi (far below Beijing).[65] Hence, together with the factor of latitude, biomass burning + lightning is a significant source of NO_x in Karachi. Although car ownership in Beijing reached 6 million in 2018, according to Chinese car industry surveys (higher than that in Karachi, at 3.6 million),

https://dx.doi.org/10.1021/acs.est.0c00490
Environ. Sci. Technol. 2020, 54, 7787−7797

the emission standards (National IV Standard) are much lower than those in Karachi (European II standard), which means that the level of pollutant gases (e.g., NO_x, SO_2) emitted by each vehicle is lower.[66] In addition, Karachi serves as a transportation hub and is home to Pakistan's two largest ports. Thus, shipping contributes a large portion of the emissions,[67] as evidenced by the results quantifying oceanic source contributions, with shipping emissions at 7.8%; this is discussed in the next section.

Karachi is home to 47% of Pakistan's industries; the major state-owned plants include Pakistani steel mills, the Karachi shipyard, and two oil refineries that consume large amounts of coal. In 2016, coal consumption in Pakistan was about 20 million tons.[68] However, the consumption was significantly lower than that in China (4.4 billion tons).[69] Although China's coal NO_x emissions have shown a downward trend due to the widespread installation of pollution control equipment, its NO_x emissions due to coal are still much higher than Pakistan's.[70] Furthermore, NO_x emissions are mainly concentrated in North China near Beijing and are prominent in winter due to residential coal burning.[71] Beijing is located on the northern edge of the North China Plain (1.3×10^6 km^2) with climatic rain and heat periods; this large agricultural area receives large amounts of nitrate fertilizer and is susceptible to fertilizer misuse.[72] Thus, a location such as this could be a significant microbial emission source. Illustratively, the NO_x contribution of this source in summer can reach about 20.8% in Beijing. In contrast, the subtropical climate around Karachi, which is almost desert-like most of the year, limits microorganism activity in this region although there are several wetland parks. These combined factors lead to the relatively lower contribution of coal combustion and microbial processes in Karachi.

Figure 3 also shows the seasonal variation in contributions from the four sources. Coal combustion exhibited the most obvious fluctuation, with a greater contribution in autumn and winter (35.5 ± 5.5%) and a smaller one in spring and summer (28.9 ± 4.8%). Biomass burning + lightning contribution changed somewhat, with high values recorded in autumn and winter. Mobile sources and microbial processes were consistent in contribution variation, showing seasonal change opposite the trends for the first two sources. Specifically, coal combustion and biomass burning + lightning peaked in October, November, and December. This was about a month before high concentrations of NO_3^- appeared, indicating that the two sources, especially coal combustion, led to the occurrence of high NO_3^- pollution in Karachi. This is consistent with the source characteristics indicated by $\delta^{15}N-NO_3^-$ findings discussed earlier. The sharp increases in coal combustion and biomass burning + lightning were in agreement with the changes in local energy demand and wind direction (SI Text S8; Figure S10), resulting in conspicuous reductions in the importance of the other two sources.[73] It is possible, of course, that the emission equivalents of the mobile sources and microbial processes did not change significantly; however, the corresponding NO_x concentrations in Karachi were not resolved in this study.

Estimation of Oceanic Contributions to NO_x. The oceanic contributions of NO_x in Karachi are still not well understood, which complicates efforts to control the air pollution in this area.[74] In this study, four trajectories were related to the AS region: two trajectories from land areas to the ocean (LO trajectory) and two from the ocean to the land (OL trajectory) (SI Figure S2). The trajectories were clustered based on the airflow trajectories over the entire sampling period, representing the interaction characteristics of the wind field between the land and the ocean.[48] As a whole, ocean-dominated air masses accounted for 69% of the total contribution, whereas 31% was due to a terrestrial trajectory.

The NO_3^- information was grouped based on the clustered trajectories (Figure 4). Mean test results indicated that the

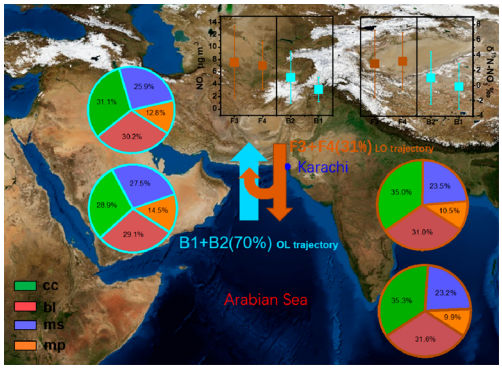

Figure 4. Characteristics of LO trajectory and OL trajectory for NO_3^- at Karachi: "F" is the forward trajectory clusters (LO trajectory), and "B" refers to the backward trajectory clusters (OL trajectory). cc, bl, ms, and mp represent the source of coal combustion, biomass burning + lightning, mobile sources, microbial processes, respectively.

NO_3^- concentration differed significantly between the OL trajectory (B1:3.2 ± 2.0 $\mu g\ m^{-3}$, B2:5.2 ± 4.2 $\mu g\ m^{-3}$) and the LO trajectory (F3:7.6 ± 5.8 $\mu g\ m^{-3}$, F4:7.0 ± 3.8 $\mu g\ m^{-3}$); the OL concentration was markedly higher than the LO concentration ($p < 0.01$), perhaps due to the dilution of the OL trajectory possessing a greater proportion. $\delta^{15}N-NO_3^-$ was +2.9 ± 4.4‰ and +3.2 ± 3.8‰ in F3 and F4, respectively, both of which were higher ($p < 0.05$) than the corresponding oceanic values of −0.1 ± 3.0‰ in B1 and +1.0 ± 3.5‰ in B2. In terms of the isotopic distributions of different sources, the contribution of coal combustion for NO_x in the LO trajectory was more obvious, consistent with its terrestrial nature.[39] Quantitatively, the contributions of coal combustion, biomass burning + lightning, mobile sources, and microbial processes in F3 and F4 were 35.0 ± 9.5%, 31.1 ± 3.4%, 23.5 ± 5.7%, and 10.5 ± 5.9% and 35.3 ± 8.2%, 31.6 ± 3.0%, 23.2 ± 5.2%, and 9.9 ± 0.5%, respectively. The source contributions to F3 and F4 showed no significant differences ($p > 0.05$), which may be due to their homology with B3, as reflected in their similar proportions (30% in B3 and 31% in F3 and F4 combined). In addition, the correlation between source contributions in the weighted integration of F3 and F4 and those in B3 was close to 1.0 (SI Figure S11), indicating that such contributions could also represent the characteristics of local terrestrial sources in Karachi.

The contributions of coal combustion in B2 and B1 were 31.1 ± 6.4% and 28.9 ± 5.2%, respectively. These contributions were reduced compared with F3 and F4; however, they were still close to 30%. A similar situation occurred with the biomass burning + lightning source, which can be explained by the effects of secondary terrestrial emissions from the near-land sea area or local terrestrial sources when the sea breeze blows. A comparison between B2 and B1 revealed that the contribution of coal combustion in B1 was lower and originated from a more distant sea area.

https://dx.doi.org/10.1021/acs.est.0c00490
Environ. Sci. Technol. 2020, 54, 7787−7797

Correspondingly, mobile sources and microbial processes were more significant in B1 (27.5 ± 3.4% and 14.5 ± 4.6%) compared with B2 (25.9 ± 4.1% and 12.8 ± 5.4%) ($p < 0.01$). Overall, the similar contributions of OL and LO trajectories suggest that most of the NO_x observed in the OL trajectory came from secondary terrestrial source contributions, and the decrease in the relative contributions from some sources was due to the addition of oceanic source contributions.

On the basis of the modeling method, the oceanic concentration of NO_3^- was estimated as 0.8 μg m^{-3}, contributing 16.8% to NO_x in the OL trajectory. This confirms the above-mentioned characteristics of the absolute contribution of terrestrial sources to NO_x in the OL trajectory. For the oceanic contribution, biomass burning + lightning, mobile sources, and microbial processes were 3.4%, 7.8%, and 5.6%, respectively. Excluding terrestrial sources (e.g., biomass burning and vehicle exhaust), the calculated 3.4% for biomass burning + lightning mostly came from lightning, and the 7.8% for mobile sources was due to shipping emissions, whereas the 5.6% portion for microbial processes was likely due to marine sediment and estuaries where the denitrification of microorganisms is vigorous. A previous study estimated that 11.3% of NO_3^- in 2013 came from ships, particularly in the Bohai and East China seas, which is higher than that calculated for Karachi in the AS region.[75] These findings are consistent with the volume of ship activity in these areas (SI Figure S12). Looking at the ocean source as a whole, lightning, shipping emissions, and microbial process sources accounted for 20.3%, 46.3%, and 33.4%, respectively, reflecting the high contribution of shipping emissions to the marine native NO_x in the AS region. Of course, it is conceivable that ships in East Asia, Europe, and North America, where ship activity is more frequent, contribute more to oceanic NO_x; thus, shipping emissions should be integrated into area air management plans to reduce pollution levels.[76]

In summary, this study assessed the oceanic contributions to NO_x emissions using nitrogen isotope analysis. This novel evaluation method is expected to have a broad application range. It is undeniable that the apportionment results may have a certain uncertainty due to the lack of source values (e.g., the absence of shipping $\delta^{15}N-NO_x$), but it is important to emphasize the dominant role of ship emissions in oceanic source contributions to the air pollution of surrounding areas.

■ ASSOCIATED CONTENT

Supporting Information

The Supporting Information is available free of charge at https://pubs.acs.org/doi/10.1021/acs.est.0c00490.

Additional materials as noted in the text (PDF)

■ AUTHOR INFORMATION

Corresponding Authors

Chongguo Tian − *CAS Key Laboratory of Coastal Environmental Processes and Ecological Remediation, Yantai Institute of Coastal Zone Research (YIC), Chinese Academy of Sciences (CAS), Yantai, Shandong 264003, P. R. China; Center for Ocean Mega-Science, Chinese Academy of Sciences, Qingdao City 266071, P. R. China;* orcid.org/0000-0001-6058-9353; Email: cgtian@yic.ac.cn

Jun Li − *State Key Laboratory of Organic Geochemistry and Guangdong Key Laboratory of Environmental Protection and Resources Utilization, Guangzhou Institute of Geochemistry, Chinese Academy of Sciences, Guangzhou 510640, China;* orcid.org/0000-0002-3637-1642; Email: junli@gig.ac.cn

Authors

Zheng Zong − *CAS Key Laboratory of Coastal Environmental Processes and Ecological Remediation, Yantai Institute of Coastal Zone Research (YIC), Chinese Academy of Sciences (CAS), Yantai, Shandong 264003, P. R. China; Center for Ocean Mega-Science, Chinese Academy of Sciences, Qingdao City 266071, P. R. China*

Jabir Hussain Syed − *Department of Meteorology, COMSATS University Islamabad (CUI), Islamabad 45550, Pakistan;* orcid.org/0000-0003-0942-8495

Wei Zhang − *School of Environmental and Material Engineering, Yantai University, Yantai, Shandong 264005, P. R. China*

Yunting Fang − *CAS Key Laboratory of Forest Ecology and Management, Institute of Applied Ecology, Chinese Academy of Sciences, Shenyang, Liaoning 110164, P. R. China;* orcid.org/0000-0001-7531-546X

Yifan Jiang − *Department of Civil and Environmental Engineering, National University of Singapore, 117575 Singapore, Singapore*

Jawad Nasir − *Earth Sciences Directorate, Pakistan Space and Upper Atmosphere Research Commission (SUPARCO), Karachi 75270, Pakistan*

Muhammad Mansha − *Earth Sciences Directorate, Pakistan Space and Upper Atmosphere Research Commission (SUPARCO), Karachi 75270, Pakistan*

Syed Hussain Haider Rizvi − *Earth Sciences Directorate, Pakistan Space and Upper Atmosphere Research Commission (SUPARCO), Karachi 75270, Pakistan*

Muhammad Shafiq − *Earth Sciences Directorate, Pakistan Space and Upper Atmosphere Research Commission (SUPARCO), Karachi 75270, Pakistan;* orcid.org/0000-0002-2570-1722

Suhaib Bin Farhan − *Earth Sciences Directorate, Pakistan Space and Upper Atmosphere Research Commission (SUPARCO), Karachi 75270, Pakistan*

Gan Zhang − *State Key Laboratory of Organic Geochemistry and Guangdong Key Laboratory of Environmental Protection and Resources Utilization, Guangzhou Institute of Geochemistry, Chinese Academy of Sciences, Guangzhou 510640, China;* orcid.org/0000-0002-9010-8140

Complete contact information is available at: https://pubs.acs.org/10.1021/acs.est.0c00490

Notes

The authors declare no competing financial interest.

■ ACKNOWLEDGMENTS

This research was financially supported by the Natural Scientific Foundation of China (NSFC; Grants 41977190 and 41907198), the NSFC-Shandong Joint Fund (U1906215), Guangdong Foundation for Program of Science and Technology Research (Grant 2017B030314057), and the International Partnership Program of Chinese Academy of Sciences (Grant No. 132744KYSB20170002). The authors gratefully acknowledge the National Oceanic and Atmospheric Administration's Air Resources Laboratory for providing the HYSPLIT transport model.

REFERENCES

(1) Galloway, J. N.; Dentener, F. J.; Capone, D. G.; Boyer, E. W.; Howarth, R. W.; Seitzinger, S. P.; Asner, G. P.; Cleveland, C. C.; Green, P. A.; Holland, E. A.; Karl, D. M.; Michaels, A. F.; Porter, J. H.; Townsend, A. R.; Vorosmarty, C. J. Nitrogen cycles: past, present, and future. *Biogeochemistry* **2004**, *70* (2), 153−226.

(2) Cheng, Y.; Zheng, G.; Wei, C.; Mu, Q.; Zheng, B.; Wang, Z.; Gao, M.; Zhang, Q.; He, K.; Carmichael, G.; Poschl, U.; Su, H. Reactive nitrogen chemistry in aerosol water as a source of sulfate during haze events in China. *Sci. Adv.* **2016**, *2* (12), No. e1601530.

(3) Fang, Y. T.; Koba, K.; Wang, X. M.; Wen, D. Z.; Li, J.; Takebayashi, Y.; Liu, X. Y.; Yoh, M. Anthropogenic imprints on nitrogen and oxygen isotopic composition of precipitation nitrate in a nitrogen-polluted city in southern China. *Atmos. Chem. Phys.* **2011**, *11* (3), 1313−1325.

(4) Wang, G.; Zhang, R.; Gomez, M. E.; Yang, L.; Zamora, M. L.; Hu, M.; Lin, Y.; Peng, J.; Guo, S.; Meng, J.; Li, J.; Cheng, C.; Hu, T.; Ren, Y.; Wang, Y.; Gao, J.; Cao, J.; An, Z.; Zhou, W.; Li, G.; Wang, J.; Tian, P.; Marrero-Ortiz, W.; Secrest, J.; Du, Z.; Zheng, J.; Shang, D.; Zeng, L.; Shao, M.; Wang, W.; Huang, Y.; Wang, Y.; Zhu, Y.; Li, Y.; Hu, J.; Pan, B.; Cai, L.; Cheng, Y.; Ji, Y.; Zhang, F.; Rosenfeld, D.; Liss, P. S.; Duce, R. A.; Kolb, C. E.; Molina, M. J. Persistent sulfate formation from London Fog to Chinese haze. *Proc. Natl. Acad. Sci. U. S. A.* **2016**, *113* (48), 13630−13635.

(5) Martin, R. V.; Jacob, D. J.; Chance, K.; Kurosu, T. P.; Palmer, P. I.; Evans, M. J. Global inventory of nitrogen oxide emissions constrained by space-based observations of NO_2 columns. *J. Geophys. Res.* **2003**, *108* (D17), 4537−4548.

(6) Fowler, D.; Coyle, M.; Skiba, U.; Sutton, M. A.; Cape, J. N.; Reis, S.; Sheppard, L. J.; Jenkins, A.; Grizzetti, B.; Galloway, J. N.; Vitousek, P.; Leach, A.; Bouwman, A. F.; Butterbach-Bahl, K.; Dentener, F.; Stevenson, D.; Amann, M.; Voss, M. The global nitrogen cycle in the twenty-first century. *Philos. Trans. R. Soc., B* **2013**, *368* (1621), No. na.

(7) Zhang, F.; Chen, Y.; Chen, Q.; Feng, Y.; Shang, Y.; Yang, X.; Gao, H.; Tian, C.; Li, J.; Zhang, G.; Matthias, V.; Xie, Z. Real-World Emission Factors of Gaseous and Particulate Pollutants from Marine Fishing Boats and Their Total Emissions in China. *Environ. Sci. Technol.* **2018**, *52* (8), 4910−4919.

(8) Corbett, J. J.; Fischbeck, P. S.; Pandis, S. N. Global nitrogen and sulfur inventories for oceangoing ships. *J. Geophys. Res.-Atmos.* **1999**, *104* (D3), 3457−3470.

(9) Ding, J.; van der A, R. J.; Mijling, B.; Jalkanen, J.-P.; Johansson, L.; Levelt, P. F. Maritime NO_x Emissions Over Chinese Seas Derived From Satellite Observations. *Geophys. Res. Lett.* **2018**, *45* (4), 2031−2037.

(10) Shimadera, H.; Kojima, T.; Kondo, A.; Inoue, Y. Performance comparison of CMAQ and CAMx for one-year $PM_{2.5}$ simulation in Japan. *Int. J. Environ. Pollut.* **2015**, *57* (3−4), 146−161.

(11) Hastings, M. G.; Steig, E. J.; Sigman, D. M. Seasonal variations in N and O isotopes of nitrate in snow at Summit, Greenland: Implications for the study of nitrate in snow and ice cores. *J. Geophys. Res.* **2004**, *109*, D20306.

(12) Liu, X. Y.; Koba, K.; Koyama, L. A.; Hobbie, S. E.; Weiss, M. S.; Inagaki, Y.; Shaver, G. R.; Giblin, A. E.; Hobara, S.; Nadelhoffer, K. J.; Sommerkorn, M.; Rastetter, E. B.; Kling, G. W.; Laundre, J. A.; Yano, Y.; Makabe, A.; Yano, M.; Liu, C.-Q. Nitrate is an important nitrogen source for Arctic tundra plants. *Proc. Natl. Acad. Sci. U. S. A.* **2018**, *115* (13), 3398−3403.

(13) Nilsson, L.; Widerlund, A. Tracing nitrogen cycling in mining waters using stable nitrogen isotope analysis. *Appl. Geochem.* **2017**, *84*, 41−51.

(14) Xiao, H. W.; Xie, L. H.; Long, A. M.; Ye, F.; Pan, Y. P.; Li, D. N.; Long, Z. H.; Chen, L.; Xiao, H. Y.; Liu, C. Q. Use of isotopic compositions of nitrate in TSP to identify sources and chemistry in South China Sea. *Atmos. Environ.* **2015**, *109*, 70−78.

(15) Eriksson, E. on the Isotopic Composition of the Ammonia and the Nitrate Ion in RaiN. *Geochim. Cosmochim. Acta* **1958**, *15* (1−2), 153−153.

(16) Freyer, H. D. Seasonal Trends of NH_4^+ and NO_3^- Nitrogen Isotope Composition in Rain Collected at Julich, GermanY. *Tellus* **1978**, *30* (1), 83−92.

(17) Freyer, H. D. Seasonal-Variation of N-15-N-14 Ratios in Atmospheric Nitrate Species. *Tellus, Ser. B* **1991**, *43* (1), 30−44.

(18) Hoering, T. The Isotopic Composition of the Ammonia and the Nitrate Ion in Rain. *Geochim. Cosmochim. Acta* **1957**, *12* (1−2), 97−102.

(19) Kamezaki, K.; Hattori, S.; Iwamoto, Y.; Ishino, S.; Furutani, H.; Miki, Y.; Uematsu, M.; Miura, K.; Yoshida, N. Tracing the sources and formation pathways of atmospheric particulate nitrate over the Pacific Ocean using stable isotopes. *Atmos. Environ.* **2019**, *209*, 152−166.

(20) Kawashima, H.; Kurahashi, T. Inorganic ion and nitrogen isotopic compositions of atmospheric aerosols at Yurihonjo, Japan: Implications for nitrogen sources. *Atmos. Environ.* **2011**, *45* (35), 6309−6316.

(21) Luo, L.; Wu, Y.; Xiao, H.; Zhang, R.; Lin, H.; Zhang, X.; Kao, S. J. Origins of aerosol nitrate in Beijing during late winter through spring. *Sci. Total Environ.* **2019**, *653*, 776−782.

(22) Song, W.; Wang, Y. L.; Yang, W.; Sun, X. C.; Tong, Y. D.; Wang, X. M.; Liu, C. Q.; Bai, Z. P.; Liu, X. Y. Isotopic evaluation on relative contributions of major NO_x sources to nitrate of $PM_{2.5}$ in Beijing. *Environ. Pollut.* **2019**, *248*, 183−190.

(23) Widory, D. Nitrogen isotopes: Tracers of origin and processes affecting PM_{10} in the atmosphere of Paris. *Atmos. Environ.* **2007**, *41* (11), 2382−2390.

(24) Elliott, E. M.; Yu, Z.; Cole, A. S.; Coughlin, J. G. Isotopic advances in understanding reactive nitrogen deposition and atmospheric processing. *Sci. Total Environ.* **2019**, *662*, 393−403.

(25) Felix, J. D.; Elliott, E. M.; Shaw, S. L. Nitrogen isotopic composition of coal-fired power plant NO_x: influence of emission controls and implications for global emission inventories. *Environ. Sci. Technol.* **2012**, *46* (6), 3528−35.

(26) Fibiger, D. L.; Hastings, M. G. First Measurements of the Nitrogen Isotopic Composition of NO_x from Biomass Burning. *Environ. Sci. Technol.* **2016**, *50* (21), 11569−11574.

(27) Miller, D. J.; Chai, J.; Guo, F.; Dell, C. J.; Karsten, H.; Hastings, M. G. Isotopic Composition of In Situ Soil NO_x Emissions in Manure-Fertilizes Cropland. *Geophys. Res. Lett.* **2018**, *45* (21), 12058−12066.

(28) Miller, D. J.; Wojtal, P. K.; Clark, S. C.; Hastings, M. G. Vehicle NO_x emission plume isotopic signatures: Spatial variability across the eastern United States. *J. Geophys. Res.-Atmos.* **2017**, *122* (8), 4698−4717.

(29) Walters, W. W.; Tharp, B. D.; Fang, H.; Kozak, B. J.; Michalski, G. Nitrogen Isotope Composition of Thermally Produced NO_x from Various Fossil-Fuel Combustion Sources. *Environ. Sci. Technol.* **2015**, *49* (19), 11363−71.

(30) Yu, Z.; Elliott, E. M. Novel Method for Nitrogen Isotopic Analysis of Soil-Emitted Nitric Oxide. *Environ. Sci. Technol.* **2017**, *51* (11), 6268−6278.

(31) Walters, W. W.; Michalski, G. Theoretical calculation of nitrogen isotope equilibrium exchange fractionation factors for various NO_y molecules. *Geochim. Cosmochim. Acta* **2015**, *164*, 284−297.

(32) Walters, W. W.; Michalski, G. Theoretical calculation of oxygen equilibrium isotope fractionation factors involving various NO_y molecules, OH, and H_2O and its implications for isotope variations in atmospheric nitrate. *Geochim. Cosmochim. Acta* **2016**, *191*, 89−101.

(33) Parnell, A. C.; Phillips, D. L.; Bearhop, S.; Semmens, B. X.; Ward, E. J.; Moore, J. W.; Jackson, A. L.; Grey, J.; Kelly, D. J.; Inger, R. Bayesian stable isotope mixing models. *Environmetrics* **2013**, *24* (6), 387−399.

(34) Lu, Y.; Lin, S.; Fatmi, Z.; Malashock, D.; Hussain, M. M.; Siddique, A.; Carpenter, D. O.; Lin, Z.; Khwaja, H. A. Assessing the association between fine particulate matter ($PM_{2.5}$) constituents and cardiovascular diseases in a mega-city of Pakistan. *Environ. Pollut.* **2019**, *252*, 1412−1422.

https://dx.doi.org/10.1021/acs.est.0c00490
Environ. Sci. Technol. 2020, 54, 7787−7797

(35) Khan, Z. Y.; Kettler, J.; Khwaja, H. A.; Naqvi, I. I.; Malik, A.; Stone, E. A. Organic Aerosol Characterization and Source Identification in Karachi, Pakistan. *Aerosol Air Qual. Res.* **2018**, *18* (10), 2550−2564.
(36) Khwaja, H. A.; Fatmi, Z.; Malashock, D.; Aminov, Z.; Kazi, A.; Siddique, A.; Qureshi, J.; Carpenter, D. O. Effect of air pollution on daily morbidity in Karachi, Pakistan. *J. Local Glob. Health Sci.* **2012**, *217*, 1−13.
(37) Liao, X.; Zhan, H.; Du, Y. Potential new production in two upwelling regions of the western Arabian Sea: Estimation and comparison. *J. Geophys. Res.: Oceans* **2016**, *121* (7), 4487−4502.
(38) Zong, Z.; Tan, Y.; Wang, X.; Tian, C.; Fang, Y.; Chen, Y.; Fang, Y.; Han, G.; Li, J.; Zhang, G. Assessment and quantification of NO_x sources at a regional background site in North China: Comparative results from a Bayesian isotopic mixing model and a positive matrix factorization model. *Environ. Pollut.* **2018**, *242*, 1379−1386.
(39) McIlvin, M. R.; Altabet, M. A. Chemical conversion of nitrate and nitrite to nitrous oxide for nitrogen and oxygen isotopic analysis in freshwater and seawater. *Anal. Chem.* **2005**, *77* (17), 5589−5595.
(40) Harrison, R. L. Introduction To Monte Carlo Simulation. *AIP Conf. Proc.* **2010**, *1204*, 17−21.
(41) Moore, J. W.; Semmens, B. X. Incorporating uncertainty and prior information into stable isotope mixing models. *Ecol. Lett.* **2008**, *11* (5), 470−480.
(42) Walters, W. W.; Simonini, D. S.; Michalski, G. Nitrogen isotope exchange between NO and NO_2 and its implications for $\delta^{15}N$ variations in tropospheric NO_x and atmospheric nitrate. *Geophys. Res. Lett.* **2016**, *43* (1), 440−448.
(43) Zong, Z.; Wang, X.; Tian, C.; Chen, Y.; Fang, Y.; Zhang, F.; Li, C.; Sun, J.; Li, J.; Zhang, G. First Assessment of NO_x Sources at a Regional Background Site in North China Using Isotopic Analysis Linked with Modeling. *Environ. Sci. Technol.* **2017**, *51* (11), 5923−5931.
(44) Heaton, E. T. H. $^{15}N/^{14}N$ rations of NO_x from vehicle engines and coal-fired power stations. *Tellus, Ser. B* **1990**, *42*, 304−307.
(45) Walters, W. W.; Goodwin, S. R.; Michalski, G. Nitrogen stable isotope composition $\delta^{15}N$ of vehicle-emitted NO_x. *Environ. Sci. Technol.* **2015**, *49* (4), 2278−85.
(46) Li, D.; Wang, X. Nitrogen isotopic signature of soil-released nitric oxide (NO) after fertilizer application. *Atmos. Environ.* **2008**, *42* (19), 4747−4754.
(47) Felix, J. D.; Elliott, E. M. Isotopic composition of passively collected nitrogen dioxide emissions: Vehicle, soil and livestock source signatures. *Atmos. Environ.* **2014**, *92*, 359−366.
(48) Bressi, M.; Sciare, J.; Ghersi, V.; Mihalopoulos, N.; Petit, J. E.; Nicolas, J. B.; Moukhtar, S.; Rosso, A.; Féron, A.; Bonnaire, N.; Poulakis, E.; Theodosi, C. Sources and geographical origins of fine aerosols in Paris (France). *Atmos. Chem. Phys.* **2014**, *14* (16), 8813−8839.
(49) Earl, D. J.; Deem, M. W. Monte Carlo simulations. *Methods Mol. Biol. (N. Y., NY, U. S.)* **2008**, *443*, 25−36.
(50) Mansha, M.; Ghauri, B.; Rahman, S.; Amman, A. Characterization and source apportionment of ambient air particulate matter ($PM_{2.5}$) in Karachi. *Sci. Total Environ.* **2012**, *425*, 176−83.
(51) Shahid, I.; Kistler, M.; Mukhtar, A.; Ghauri, B. M.; Ramirez-Santa Cruz, C.; Bauer, H.; Puxbaum, H. Chemical characterization and mass closure of PM_{10} and $PM_{2.5}$ at an urban site in Karachi − Pakistan. *Atmos. Environ.* **2016**, *128*, 114−123.
(52) Shahid, I.; Alvi, M. U.; Shahid, M. Z.; Alam, K.; Chishtie, F. Source Apportionment of PM_{10} at an Urban Site of a South Asian Mega City. *Aerosol Air Qual. Res.* **2018**, *18* (9), 2498−2509.
(53) An, Z.; Huang, R.-J.; Zhang, R.; Tie, X.; Li, G.; Cao, J.; Zhou, W.; Shi, Z.; Han, Y.; Gu, Z.; Ji, Y. Severe haze in northern China: A synergy of anthropogenic emissions and atmospheric processes. *Proc. Natl. Acad. Sci. U. S. A.* **2019**, *116* (18), 8657−8666.
(54) Hastings, M. G.; Jarvis, J. C.; Steig, E. J. Anthropogenic impacts on nitrogen isotopes of ice-core nitrate. *Science* **2009**, *324* (5932), 1288.
(55) Song, W.; Liu, X.-Y.; Wang, Y.-L.; Tong, Y.-D.; Bai, Z.-P.; Liu, C.-Q. Nitrogen isotope differences between atmospheric nitrate and corresponding nitrogen oxides: A new constraint using oxygen isotopes. *Sci. Total Environ.* **2020**, *701*, 134515.
(56) Alexander, B.; Hastings, M. G.; Allman, D. J.; Dachs, J.; Thornton, J. A.; Kunasek, S. A. Quantifying atmospheric nitrate formation pathways based on a global model of the oxygen isotopic composition (ΔO^{17}) of atmospheric nitrate. *Atmos. Chem. Phys.* **2009**, *9* (14), 5043−5056.
(57) Elliott, E. M.; Kendall, C.; Boyer, E. W.; Burns, D. A.; Lear, G. G.; Golden, H. E.; Harlin, K.; Bytnerowicz, A.; Butler, T. J.; Glatz, R. Dual nitrate isotopes in dry deposition: Utility for partitioning NO_x source contributions to landscape nitrogen deposition. *J. Geophys. Res.* **2009**, *114*, G04020.
(58) Ahern, A. T.; Goldberger, L.; Jahl, L.; Thornton, J.; Sullivan, R. C. Production of N_2O_5 and $ClNO_2$ through Nocturnal Processing of Biomass-Burning Aerosol. *Environ. Sci. Technol.* **2018**, *52* (2), 550−559.
(59) Lu, K.; Fuchs, H.; Hofzumahaus, A.; Tan, Z.; Wang, H.; Zhang, L.; Schmitt, S. H.; Rohrer, F.; Bohn, B.; Broch, S.; Dong, H.; Gkatzelis, G. I.; Hohaus, T.; Holland, F.; Li, X.; Liu, Y.; Liu, Y.; Ma, X.; Novelli, A.; Schlag, P.; Shao, M.; Wu, Y.; Wu, Z.; Zeng, L.; Hu, M.; Kiendler-Scharr, A.; Wahner, A.; Zhang, Y. Fast Photochemistry in Wintertime Haze: Consequences for Pollution Mitigation Strategies. *Environ. Sci. Technol.* **2019**, *53* (18), 10676−10684.
(60) Xue, L.; Wang, T.; Louie, P. K. K.; Luk, C. W. Y.; Blake, D. R.; Xu, Z. Increasing External Effects Negate Local Efforts to Control Ozone Air Pollution: A Case Study of Hong Kong and Implications for Other Chinese Cities. *Environ. Sci. Technol.* **2014**, *48* (18), 10769−10775.
(61) Iqbal, M.; Syed, J. H.; Breivik, K.; Chaudhry, M. J. I.; Li, J.; Zhang, G.; Malik, R. N. E-Waste Driven Pollution in Pakistan: The First Evidence of Environmental and Human Exposure to Flame Retardants (FRs) in Karachi City. *Environ. Sci. Technol.* **2017**, *51* (23), 13895−13905.
(62) Alam, K.; Rahman, N.; Khan, H. U.; Haq, B. S.; Rahman, S. Particulate Matter and Its Source Apportionment in Peshawar, Northern Pakistan. *Aerosol Air Qual. Res.* **2015**, *15* (2), 634−647.
(63) Alam, K.; Trautmann, T.; Blaschke, T.; Majid, H. Aerosol optical and radiative properties during summer and winter seasons over Lahore and Karachi. *Atmos. Environ.* **2013**, *74*, 412−412.
(64) Lodhi, A.; Ghauri, B.; Khan, M. R.; Rahman, S.; Shafique, S. Particulate Matter ($PM_{2.5}$) Concentration and Source Apportionment in Lahore. *J. Braz. Chem. Soc.* **2009**, *20* (10), 1811−1820.
(65) Chen, F.; Lao, Q.; Jia, G.; Chen, C.; Zhu, Q.; Zhou, X. Seasonal variations of nitrate dual isotopes in wet deposition in a tropical city in China. *Atmos. Environ.* **2019**, *196*, 1−9.
(66) *China Statistical Yearbook, Part XVI: Transport, Post, And Telecommunication Services*; China Statistics Press: Beijing, China, 2017.
(67) Ramacher, M. O. P.; Karl, M.; Bieser, J.; Jalkanen, J.-P.; Johansson, L. Urban population exposure to NO_x emissions from local shipping in three Baltic Sea harbour cities − a generic approach. *Atmos. Chem. Phys.* **2019**, *19* (14), 9153−9179.
(68) Rehman, S. A. U.; Cai, Y.; Mirjat, N. H.; Das Walasai, G.; Shah, I. A.; Ali, S. The Future of Sustainable Energy Production in Pakistan: A System Dynamics-Based Approach for Estimating Hubbert Peaks. *Energies* **2017**, *10*, 1858.
(69) *China Statistical Yearbook, Part IX: Energy*; China Statistics Press: Beijing, China, 2017.
(70) Liu, F.; Beirle, S.; Zhang, Q.; van der A, R. J.; Zheng, B.; Tong, D.; He, K. NO_x emission trends over Chinese cities estimated from OMI observations during 2005 to 2015. *Atmos. Chem. Phys.* **2017**, *17* (15), 9261−9275.
(71) Zong, Z.; Tan, Y.; Wang, X.; Tian, C.; Li, J.; Fang, Y.; Chen, Y.; Cui, S.; Zhang, G. Dual-modelling-based source apportionment of NO_x in five Chinese megacities: Providing the isotopic footprint from 2013 to 2014. *Environ. Int.* **2020**, *137*, 105592−105592.

https://dx.doi.org/10.1021/acs.est.0c00490
Environ. Sci. Technol. 2020, 54, 7787−7797

(72) Ning, J.; Liu, J.; Kuang, W.; Xu, X.; Zhang, S.; Yan, C.; Li, R.; Wu, S.; Hu, Y.; Du, G.; Chi, W.; Pan, T.; Ning, J. Spatiotemporal patterns and characteristics of land-use change in China during 2010−2015. *J. Geogr. Sci.* **2018**, *28* (5), 547−562.
(73) Colbeck, I.; Nasir, Z. A.; Ali, Z. The state of ambient air quality in Pakistan–a review. *Environ. Sci. Pollut. Res.* **2010**, *17* (1), 49−63.
(74) Zhang, X.; Zhang, Y.; Liu, Y.; Zhao, J.; Zhou, Y.; Wang, X.; Yang, X.; Zou, Z.; Zhang, C.; Fu, Q.; Xu, J.; Gao, W.; Li, N.; Chen, J. Changes in the SO_2 Level and $PM_{2.5}$ Components in Shanghai Driven by Implementing the Ship Emission Control Policy. *Environ. Sci. Technol.* **2019**, *53* (19), 11580−11587.
(75) Zhang, F.; Chen, Y.; Tian, C.; Lou, D.; Li, J.; Zhang, G.; Matthias, V. Emission factors for gaseous and particulate pollutants from offshore diesel engine vessels in China. *Atmos. Chem. Phys.* **2016**, *16* (10), 6319−6334.
(76) Corbett, J. J.; Winebrake, J. J.; Green, E. H.; Kasibhatla, P.; Eyring, V.; Lauer, A. Mortality from ship emissions: A global assessment. *Environ. Sci. Technol.* **2007**, *41* (24), 8512−8518.

https://dx.doi.org/10.1021/acs.est.0c00490
Environ. Sci. Technol. 2020, 54, 7787−7797